I&EC research
Industrial & Engineering Chemistry Research

Article

pubs.acs.org/IECR

# Trends in Thermoresponsive Behavior of Lipophilic Polymers

Priyanka Bhattacharya,[‖,†] Uma Shantini Ramasamy,[‡] Susan Krueger,[§] Joshua W. Robinson,[†,⊥] Barbara J. Tarasevich,[†] Ashlie Martini,[‡] and Lelia Cosimbescu*[,†]

[†]Energy and Environment Directorate, Pacific Northwest National Laboratory, 902 Battelle Boulevard, Richland, Washington 99354, United States

[‡]School of Engineering, University of California-Merced, Merced, California 95343, United States

[§]NIST Center for Neutron Research, NIST, 100 Bureau Drive, Stop 8562, Gaithersburg, Maryland 20899-8562, United States

Supporting Information

**ABSTRACT:** In an effort to find correlations between size changes with temperature of lipophilic polymers in solution and viscosity index trends, the determination of the size of thermoresponsive polymers of various architectures (linear, comb-like, star, and hyperbranched) using two experimental techniques under infinite dilution conditions (0.5% w/w) − dynamic light scattering and small angle neutron scattering, and predictive molecular dynamics simulations is described herein. Viscosity index is an important parameter for lubricants and other rheological applications. The aim of this work was to predict polymer behavior as viscosity index improvers (VIIs) using tools which require minimal amounts of material, as opposed to measuring kinematic viscosities, which require multigram quantities. There were no significant correlations between changes in polymer size with temperature and viscosity index (VI). The polymers with the highest VI (polyalkyl methacrylate - PAMA and Star PAMA) had polar backbones in contrast to the nonpolar backbones of the linear and hyperbranched (OCP and HBPE, respectively), so the disparity in solubility of the backbone and solvent medium appears to correlate with the observed VIs. It was concluded that none of the aforementioned techniques can entirely predict the polymer behavior as VIIs, at least in the temperature range studied (40−100 °C).

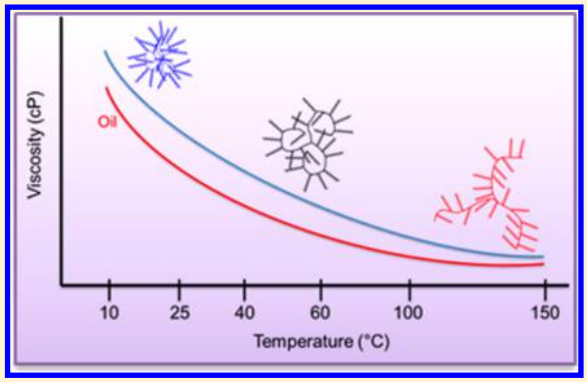


## 1. INTRODUCTION

Viscosity modifiers (VMs) or viscosity index improvers (VIIs) are additives used in lubricating oils and greases to mitigate the natural fluids' loss of viscosity with temperature. The higher the viscosity index (VI), the smaller the change in viscosity with temperature is observed. In other words, the VI is an arbitrary measure for the change of viscosity of fluids with variations in temperature and therefore a measure of the additive's efficiency at resisting thinning with temperature.

These additives are mainly polymers of various chemical compositions and architectures. Among the several polymeric VMs previously explored,[1−6] two widespread examples include the following: 1) olefin copolymers (OCP) which are fully saturated, lipophilic, nonpolar, carbon based polymers that thicken oils and 2) poly(alkyl methacrylate)s (PAMA) which include fatty pendants and polar esters within the polymer chain, with lipophilic side chains but somewhat polar backbone.[3,7] The differing chemical compositions and architectures of these VMs translate into unique viscosity performance properties which have been exploited for certain lubricant applications. In particular, PAMAs tend to be better VIIs in part due to a lower lubricant thickening effect at lower temperatures and potentially a greater solvation difference at hot versus cold temperatures.

The widely accepted mechanism of VII's thermoresponsive nature revolves around the notion of polymer coil expansion at high temperatures and promotion of a globular conformation at low temperature;[8,9] however, the mechanism of the VII's size change with temperature has only been empirically understood and directly investigated once before.[8] The intrinsic viscosity of a polymer, which relates to its radius of gyration ($R_g$), is temperature dependent.[10−12] Techniques to elucidate the functional mechanisms for the change in polymer size of thermoresponsive polymers have traditionally included dynamic light scattering (DLS)[13,14] and small angle neutron scattering (SANS).[8,15,16] DLS and SANS are perhaps two of the most complementary methods to measure temperature induced structural changes of polymers in solution. While DLS provides the hydrodynamic size ($R_h$) of the polymers in a solution, SANS gives information on the specific polymer coil transitions and is considered to be a direct measure of polymer dimensions, i.e. radius of gyration ($R_g$). Covitch and Trickett recently showed, using SANS measurements, that PAMA based

**Received:** September 30, 2016
**Revised:** November 17, 2016
**Accepted:** December 1, 2016
**Published:** December 1, 2016





DOI: 10.1021/acs.iecr.6b03812
Ind. Eng. Chem. Res. 2016, 55, 12983−12990

VIIs undergo a transition from Gaussian coil to a coil experiencing excluded volume interactions with increasing temperatures in *d*-dodecane.[8]

The work herein probes the theorized connection between VI values and molecular expansion with temperature for various polymer architectures, including linear, comb, star, and hyperbranched. We attempted to identify qualitatively, a predictive tool for VII performance of oil soluble polymers with unique architectures and chemical compositions. To this end, we explored physical techniques, SANS and DLS, and a predictive model, molecular dynamics (MD) simulation, to identify trends between dimensional changes and VII performance. Viscosity measurements for VI determination typically require multigram quantities of a given polymer which can be quite expensive to synthesize. The present methodologies only require milligram quantities (5 mg) for screening and therefore would provide a much faster result. So, in addition to challenging the conventional wisdom, finding a trend would offer a great benefit to researchers in the field of polymeric lubricant additives.

## 2. EXPERIMENTAL SECTION

**2.1. Materials and VI Determination.** The VII polymers highly branched poly(ethylene)s (HBPE)[17] and star poly(dodecyl methacrylate) (Star)[18] were prepared as previously described in the literature, whereas OCP and PAMA are proprietary materials obtained from industrial collaborators. These polymers were separately dissolved into Yubase4 (4Y) base oil at various concentrations (Table 1). The dynamic viscosities of these solutions were measured by a Brookfield spindle viscometer at 40 and 100 °C. Kinematic viscosities were determined by dividing dynamic viscosity by the density of the solution (0.83 g/mL). The densities were determined on an analytical balance with 10 mL volumetric flasks at room temperature. VI values were calculated via a widely accepted ASTM D2270, a standard practice for calculating VI from measured KV40 and KV100 values. The concentrations of the solutions for VI calculation were adjusted accordingly until KV100s were equivalent.

**Table 1. Kinematic Viscosities and Viscosity Index Values at Different Concentrations**

| parameters[a] | 4Y | OCP | HBPE | Star | PAMA |
|---|---|---|---|---|---|
| concentration (wt %) | na | 2 | 2 | 2 | 2 |
| KV40 (cSt) | 18.8 | 100.8 | 40.5 | 30.4 | 33.3 |
| KV100 (cSt) | 4.2 | 17.2 | 8.2 | 7.0 | 8.2 |
| VI | 127.0 | 187.8 | 185.6 | 205.0 | 239.0 |
| concentration (wt %) | na | 0.8 | 2.0 | 2.8 | 2.0 |
| KV40 when KV100 = 8.3 cSt | 18.8 | 42.1 | 40.2 | 35.6 | 33.9 |
| KV100 (cST) | 4.2 | 8.4 | 8.4 | 8.3 | 8.4 |
| VI at matched KV100 | 127.0 | 181.0 | 190.0 | 221.0 | 238.0 |

[a]Errors in concentration and VI values are within ±5%.

**2.2. Dynamic Light Scattering (DLS).** DLS measurements were performed in a Brookhaven ZetaPALS 90 Plus particle size analyzer equipped with a temperature controller and a 35 mW red diode laser with a nominal 640 nm wavelength. All measurements were collected at 90° scattering angle. Polymers were dissolved in hexadecane at 0.5 wt % (infinite dilution) and then centrifuged at 13,000 rpm for 20 min to remove large aggregates (≈6000 nm diameter) to improve the autocorrelation function (ACF). The polymer solutions were loaded into square quartz cells with Teflon tops and sealed with Parafilm tape to prevent any solvent evaporation. Temperature ramping was carried out from 25 to 95 °C in steps of 10 °C. The samples were equilibrated for 30 min before taking measurements at each temperature. The average diameters were determined with temperature corrected solvent viscosities.[19] Errors in the measurements were calculated based on the standard error of the mean between 3 to 5 runs.

**2.3. Small Angle Neutron Scattering (SANS).** For SANS experiments, polymer samples were dissolved in *d*-hexadecane at mass fraction of 0.5 (wt %), same concentration as DLS measurements, and run at 25, 40, 70, and 100 °C. SANS measurements were performed on the NG7 30 m SANS instrument at the NIST Center for Neutron Research (NCNR) in Gaithersburg, Maryland.[20] The neutron wavelength, $\lambda$, was 6 Å, with a wavelength spread, $\Delta\lambda/\lambda$, of 0.15. Scattered neutrons were detected with a 64 × 64 cm$^2$ two-dimensional, position-sensitive detector with 128 × 128 pixels at a resolution of 0.5 cm/pixel. Data reduction was accomplished using Igor Pro software (WaveMetrics, Lake Oswego, OR) with SANS data reduction macros developed at the NCNR.[21] Raw counts were normalized to a common monitor count and then corrected for empty cell counts, ambient room background counts, and nonuniform detector response. Data were placed on an absolute scale by normalizing the scattering intensity to the incident beam flux for each individual pixel. Finally, the data were radially averaged to produce the scattering intensity $I(q)$ versus $q$ curves, where $q = 4\pi\sin(\theta)/\lambda$ and $2\theta$ is the scattering angle measured from the axis of the incoming neutron beam. Sample-to-detector distances of 13.0, 4.0, and 1.0 m were used in order to cover the range of $0.004 \leq q \leq 0.55$ Å$^{-1}$. The $I(q)$ versus $q$ scattering data obtained at the two instrument configurations were merged using the NCNR SANS reduction software.[21]

SANS data were fit to the Polymer Excluded Volume function[22,23] using Igor Pro (WaveMetrics, Lake Oswego, OR) with SANS data analysis macros developed at the NCNR[21] in order to determine the $R_g$ and the Porod exponent, $n$, that describes the overall size and morphology of the polymer. In cases where the Polymer Excluded Volume function did not fit the data at low $q$ values (meaning that the overall $R_g$ was too large to be measured with SANS), the data were also fit using the Correlation Length function, which is an empirical formula that enables the determination of a correlation length, $L_c$, that essentially describes the interactions of the polymer chains with the solvent and the determination of a Porod exponent.[24]

Certain commercial equipment, instruments, or materials are identified in this paper to foster understanding. Such identification does not imply recommendation or endorsement by the National Institute of Standards and Technology, nor does it imply that the materials or equipment identified are necessarily the best available for the purpose.

**2.4. Molecular Dynamics (MD) Simulations.** The simulation systems created had periodic boundaries in all three directions, and the size of the simulation box was either 6 × 6 × 6 nm$^3$ (PAMA, OCP, and HBPE) or 7 × 7 × 7 nm$^3$ (Star). As illustrated in Figure S2 (a) for HBPE, each respective polymer was placed in the virtual dodecane solvent. Initial simulation structures were constructed with Accelrys Materials Studio and subsequent simulations performed using Large Atomic/Molecular Massively Parallel Simulation (LAMMPS) software.[25] The All Atom Optimized Potential for Liquid


DOI: 10.1021/acs.iecr.6b03812
Ind. Eng. Chem. Res. 2016, 55, 12983−12990

Scheme 1. Schematic Representation of the Four Analogs Investigated, Where the Red Line Represents the Polar Backbone

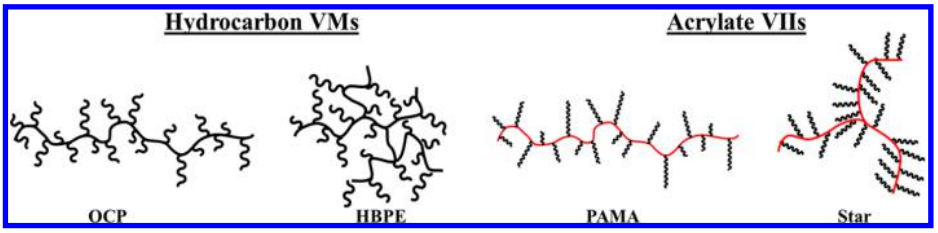


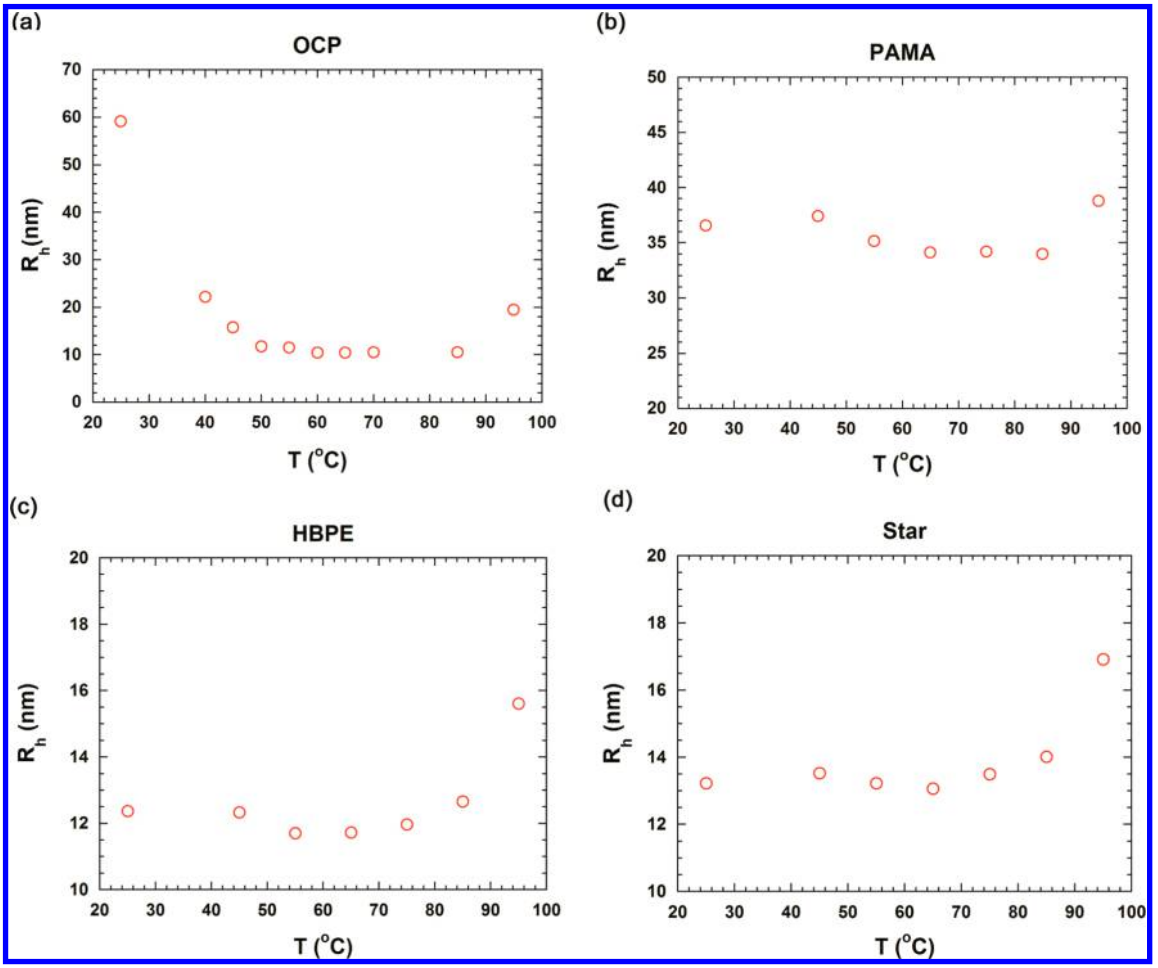


**Figure 1.** DLS plots as a function of temperature for (a) OCP, (b) PAMA, (c) HBPE, and (d) Star polymers. The scales of the *y*-axes have been adjusted to better visualize the changes in $R_h$. Error bars (standard error of the mean over 3 to 5 sample runs) are smaller than the data points and are not shown for clarity.

Simulations (OPLS-AA) force field[26] with a global cutoff of 1.2 nm was used to describe bond, angle, torsion, and nonbonded interactions between all atoms. A Nośe-Hoover thermostat and barostat maintained the temperature and pressure of the system. All simulations were run with a time step of 1 fs and a 1 to 4 intramolecular scaling factor of 0.0. Setting the scaling factor to zero turns off the van der Waals and Coulombic interactions between 1 and 4 atom pairs, which are those separated by three bonds, and has been shown to increase the prediction accuracy of liquid-state properties for molecules with 12 carbons or more.[27]

The simulations were divided into three phases: relaxation, equilibration, and production. During the relaxation stage, simulations were run at high temperatures under NVT conditions (constant number of atoms, volume, and temperature) to rapidly relax the system. The system was then equilibrated under NPT conditions (constant number of atoms, pressure, and temperature) at 40 and 100 °C, respectively, without data collection. Finally, during the production phase, the system continued to run under NPT conditions, while information on the polymer's coil size was collected for analysis. Details on the simulation stages can be found in ref 28.

Radius of gyration, $R_g$, is frequently used to quantify a polymer's coil size. In MD simulations, $R_g$ is defined as the mass weighted average distance from the center of mass of the molecule to each atom in the molecule. Here, $R_g$ was calculated at every 5 ps interval during the production stage, and the data then was used to plot frequency histograms. The frequency histograms essentially map the recurrence of specific conformations throughout the simulation time. A Gaussian function was fit to the frequency histogram to quantify the mean, $\mu$, of the distribution. This is illustrated for HBPE in


DOI: 10.1021/acs.iecr.6b03812
Ind. Eng. Chem. Res. 2016, 55, 12983−12990

Figure S2 (b). Lastly, the percent change in coil size with temperature was calculated from the mean of the coil size distribution at 40 and 100 °C using $(\mu_{100\ °C} - \mu_{40\ °C})/\mu_{40\ °C} \times 100$.

## 3. RESULTS

**3.1. Viscosity Index of Polymers.** Four VIIs were selected for this study to include variations in architecture and chemical composition (Scheme 1). OCPs are hydrocarbon based linear polymers that are soluble in Group III oils and nonpolar solvents. They generally have short alkyl side-chains extending from the polymer backbone. HBPEs have a similar chemical composition to OCPs but differ in architecture. HBPEs have a random branch-on-branch configuration that limits conformational mobility.[17] PAMAs are generally comb-like polymers with a relatively polar backbone (i.e., ester) and lipophilic side chains, which vary in polarity, length, and branching. Viscosity performance and therefore coil expansion with PAMAs are typically accredited to the oil immiscible repeating units which, presumably, repel hydrocarbons at low temperatures but allow diffusion at elevated temperatures. Star, like PAMAs, contains a lipophilic pendant group (i.e., $C_{12}$) extending from a polar backbone but has three arms connected to a center moiety that inherently limits conformational freedom. It is important to note that all four analogs have different molecular weights and therefore unique hydrodynamic volumes. For this reason, we tried to identify a relationship between VI performance and the percent change in the dimensions of these polymers.

The VI values of the four analogs were determined from kinematic viscosities (KV) of their oil solutions (Yubase-4, 4Y) at 40 and 100 °C. Initially, a 2% by weight (w/w) concentration was screened, and then the concentrations were adjusted so that the kinematic viscosities of all solutions were the same at 100 °C (KV100). The KV values of the adjusted concentrations at 40 and 100 °C were utilized to calculate the respective VIs via an online calculator (Uniteasy Calculation of Viscosity Index www.uniteasy.com/en/unitsCon/calvi.htm). The calculator has a built in algorithm which generates VIs based on the KV values input. All measurements were repeated to ensure accuracy. The corresponding VI values are reported in Table 1.

**3.2. DLS Measurements of Temperature-Responsiveness of Polymers.** The hydrodynamic radii ($R_h$) of the polymers in hexadecane (0.5 wt % polymers in solution) were measured stepwise between 25 and 95 °C. Hexadecane was chosen as the solvent due to a desirable boiling point (286.8 °C) and heat capacity (499.72 $JK^{-1}$ $mol^{-1}$) as well as chemical similarity to petroleum base oils (i.e., saturated alkane). The results are shown in Figure 1 (a)-(d) and summarized in Table 2. The $R_h$ values were mean sizes obtained by cumulant analysis. All polymers, except for OCP, had an average $R_h$ between 10 and 35 nm at 25 °C. It is possible a few large aggregates remained in the OCP solution despite extensive filtering, resulting in one outlier point of $R_h \approx 60$ nm at 25 °C.

OCP showed a continuous decrease in $R_h$ with temperature, with a plateau between 65 and 85 °C and an increase in $R_h$ at 95 °C. PAMA showed a moderate decrease in size until about 75 °C and a slight increase at the highest T (95 °C). Like OCP, both HBPE and Star polymers show an increase in size from 65 to 95 °C. These trends can be seen clearly from the percent change in size of the polymers between $T$ = 45 and 95 °C (Table 2). A negative percent change indicates a decrease in polymer size, whereas a positive percent supports an increase in polymer size with rising temperatures. The percent increase in size of the HBPE and Star polymers are similar, although they behave somewhat differently as VIIs within the temperature window of study. It is notable that the chemical composition and molecular weights of PAMAs may significantly vary, depending on the source; therefore, the magnitude of the trend in polymer size may differ as well. The polymer dimensions in solution will depend on the interactions between the like and unlike components of the solvent and the polymer segments, which in turn determine whether the polymer intrasegmental interactions are more preferred over interactions with solvent molecules. Hence, better the solvent (i.e., good solvents), greater is the swelling in the polymer. In good solvents, as temperature increases, the polymer−solvent interaction increases while the polymer−polymer (intra- and intermolecular) interaction decreases thereby resulting in coil expansion.[29] When the concentration of the polymer solution is infinitely dilute, intermolecular polymer−polymer interactions are negligible. Therefore, any change in the intrinsic viscosity of the solution at such low concentrations may be attributed to the polymer−solvent interaction. An independence of the polymer size on temperature may indicate that either the solvent behaves as a good solvent throughout the temperature range in this study or that the polymer coil does not expand while increasing temperature. A decrease in polymer size, however, indicates polymer coil contraction and suggests the polymer−solvent interaction is less favorable at elevated temperatures. The temperature range of these experiments may not be all inclusive toward studying polymer coil expansion or the more elusive globule-to-coil polymer transition state but does provide a qualitative understanding of the relationship between changes in polymer size and VI behavior. Overall, there appears to be no correlation between $\Delta R_h$ and VI values based on DLS measurements.

**3.3. SANS Results of Temperature-Responsive Polymers in *d*-Hexadecane.** While DLS provides information on the global topology of the polymers and their solvent interactions, SANS provides a direct measure of polymer dimensions and internal structure. Our experiments were conducted with polymer samples dissolved in *d*-hexadecane at 0.5 wt % at 25, 40, 70, and 100 °C. *d*-Hexadecane is considered a good base oil mimic.[8] Figure 2 shows the SANS profiles for the four polymer solutions measured at 40 and 100 °C. The scattering from the solvent has been subtracted. The overall scattering decreased as a function of temperature for all four polymers. Differences in the shape of the scattering curves as a function of temperature were more subtle and were deduced through model fitting. The high-Q region, or the Porod region, contains information on the local structure of the polymers. The $I(q)$ values at mid and low Q regions nearly overlapped for all polymers at both temperatures, as expected at infinite dilute conditions. The plots representing $I(q)$ data in Figure 2 hence

**Table 2. Summary of DLS Measurements for All Polymers at 45 and 95 °C**

| parameters[a] | OCP | HBPE | Star | PAMA |
|---|---|---|---|---|
| VI at matched KV100 | 181 | 190 | 221 | 238 |
| Rh_45 °C (nm) | 15.82 | 12.33 | 13.53 | 37.44 |
| $R_h$_95 °C (nm) | 19.50 | 15.613 | 16.92 | 38.79 |
| $\Delta R_h = [R_{h95} - R_{h45}]/R_{h45}$ (%) | +23.26 | +26.62 | +25.05 | +3.61 |

[a]Errors in VI values are within ±5%. Errors (standard error of the mean over 3−5 sample runs) in $R_h$ are within ±0.04 nm.



DOI: 10.1021/acs.iecr.6b03812
Ind. Eng. Chem. Res. 2016, 55, 12983−12990

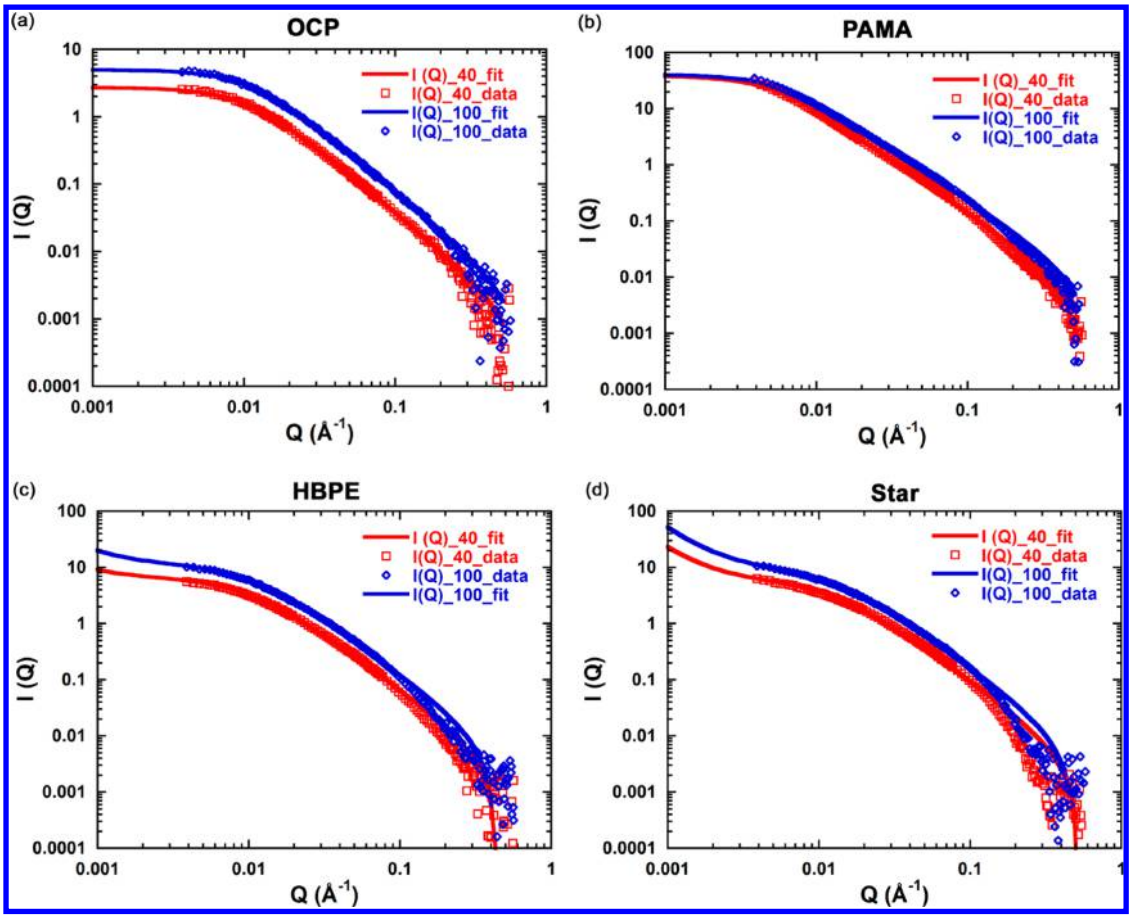


**Figure 2.** SANS profiles of (a) OCP, (b) PAMA, (c) HBPE, and (d) Star polymers in *d*-hexadecane. Solid red and blue lines show model fits to the SANS data. The data for OCP and PAMA polymers have been fitted to the polymer excluded volume model, whereas data for HBPE and Star polymers have been fitted to the correlation length model. The $I(Q)$ values at 100 °C data and their corresponding fits in each plot have been multiplied by 2 for clarity. Error bars (standard error of the mean for the number of detector pixels used in the data averaging) at low $Q$ are smaller than the data points, and error bars at high $Q$ are not shown for clarity.

**Table 3. Summary of SANS Results for All Polymers at 40 and 100 °C**

| sample ($T$ °C) | model fit | Porod exponent,[a] $n$ | $R_g$[a] (nm) | $\Delta R_g$ $[R_{g100}-R_{g40}]/R_{g40}$ (%) |
|---|---|---|---|---|
| OCP (40 °C) | polymer excluded volume | 1.85 ± 0.01 | 13.6 ± 0.1 | |
| OCP (100 °C) | polymer excluded volume | 1.85 ± 0.01 | 13.0 ± 0.1 | −4.4 ± 1.0 |
| PAMA (40 °C) | polymer excluded volume | 1.87 ± 0.01 | 27.8 ± 0.1 | |
| PAMA (100 °C) | polymer excluded volume | 1.78 ± 0.01 | 24.3 ± 0.1 | −12.6 ± 1.8 |
| sample ($T$ °C) | model fit | Porod exponent, $n$ | correlation length[a] $L_c$ (nm) | $\Delta L_c$ $[L_{c100}]-L_{c40}-/L_{c40}$ (%) |
| HBPE (40 °C) | correlation length | 1.90 ± 0.01 | 10.4 ± 0.1 | |
| HBPE (100 °C) | correlation length | 1.90 ± 0.01 | 10.5 ± 0.1 | +0.96 ± 1.37 |
| Star (40 °C) | correlation length | 2.10 ± 0 0.01 | 8.2 ± 0.1 | |
| Star (100 °C) | correlation length | 2.10 + 0.01 | 8.0 ± 0.1 | −2.43 ± 3.20 |

[a]Errors in $R_g$, $L_c$, and the Porod exponent are the statistical errors determined from the fits to the data.

have been multiplied by a factor of 2 for clarity. OCP and PAMA polymers fit well to the polymer excluded volume interactions model with Porod exponents ($n$) close to 5/3. This indicates the polymer coils are swollen and in good solvent conditions. However, both HBPE and Star polymers had Porod exponents closer to 2, validating their compact conformation by design and indicating Gaussian chain structures. Furthermore, they did not fit well with the polymer excluded volume interactions model nor the Gaussian coil or Debye models. Hence, an empirical model with Porod and Lorentzian-like terms was used, to get the correlation lengths ($L_c$) and Porod exponents to fit the scattering curves for these polymers. The comparisons between the polymer excluded volume interactions model and the correlation length model fits are shown in the Supporting Information (Figure S3) for HBPE and the Star polymers. Using the correlation length model, no reduction in $n$ or change in $R_g$ with increasing temperature was observed for the Star and HBPE polymers, implying that their internal flexibility is low. Even though HBPE and Star polymers fit poorly to the polymer excluded volume model, the Porod values computed were similar to those from the correlation length model, and $R_g$ showed the same trends as the correlation length (Table S1). On the other hand, a very minor reduction in $n$ from 1.87 (40 °C) to 1.78 (100 °C) was


DOI: 10.1021/acs.iecr.6b03812
Ind. Eng. Chem. Res. 2016, 55, 12983−12990

observed for PAMA suggesting a coil experiencing excluded volume interactions with increasing temperature. This change is also accompanied by a slight decrease in $R_g$. The results of the fits are shown in Table 3.

The $R_g$ and $L_c$ values determined by SANS are smaller than the $R_h$ values determined by DLS. The DLS method probes the diffusion behavior of the polymer, while the SANS method detects inhomogeneities in the neutron density of a sample. The hydrodynamic radius determined by DLS will include associated solvent that is not visible to SANS. The SANS method, therefore, will tend to measure the polymer size and will show a significant change in polymer dimensions only if there is a structural change in the polymer with changing temperature, while DLS measures the size of the polymer plus associated solvent.[30]

**3.4. MD Predictions of Temperature-Dependent Size Change of Polymers in Dodecane.** The third method used to characterize polymer change in size with temperature was MD simulations of each model polymer in dodecane (Figure S1). For each polymer, a maximum of 50 repeat units was chosen as the polymer length as a compromise between computational efficiency and realism. With this length basis, the model PAMA has a molecular mass of 12722.7 g/mol, OCP has a mass of 1755.39 g/mol, and HBPE has a mass of 3831.39 g/mol. The model Star polymer has 16 repeat units in each arm (a total of 48 repeat units in all three arms) and a mass of 12584.4 g/mol. The evolution of the polymer's coil size, determined by the radius of gyration, $R_g$, was observed throughout the simulation duration.

Table 4 summarizes mean $R_g$ values calculated from MD simulations at 40 and 100 °C and the percent change in coil size with temperature for all four molecules described above. Like the DLS and SANS results, a positive percent change indicates coil size expansion, while a negative percent change implies coil size contraction with temperature. From Table 4, we observe that PAMA is the only molecule that is predicted to expand significantly with temperature. OCP, HBPE, and Star, on the other hand, exhibit similar mean $R_g$ values at both temperatures, suggesting that these polymers undergo negligible changes in coil size with temperature.

**Table 4. Mean Values of the $R_g$ Distribution for All Polymers at 40 and 100 °C along with the Percent Change in Coil Size with Temperature**[a]

| temp (°C) | OCP[31] (nm) | HBPE (nm) | Star (nm) | PAMA[31] (nm) |
|---|---|---|---|---|
| 40 | 1.65 | 1.72 | 2.15 | 1.71 |
| 100 | 1.61 | 1.73 | 2.10 | 2.25 |
| % change | −2.4 | 0.18 | −2.3 | 31.5 |

[a]Data for PAMA and OCP are from ref 31.

## 4. DISCUSSION

A summary of the results from DLS, SANS, and MD is shown in Figure 3. Comparing the simulation calculations to the SANS experimental measurements, we observed an opposite trend, with the exception of PAMA, where a decrease in size was observed in SANS measurements. However, through our DLS measurements, we observed a significant increase in size with temperature for the OCP, HBPE, and Star polymers and a modest increase in size of PAMA with temperature. Simulations entirely disagree with DLS, where a significant increase in size with temperature is observed for all analogs, except for PAMA. However, considering that PAMA has the highest VI, followed by the Star, then HBPE and OCP simulations, do predict realistically PAMA's behavior.

The DLS data shows that OCP, HBPE, and Star clearly expand with temperature, while SANS shows the opposite effect. As mentioned earlier, DLS can detect the solvent shell associated with the polymer, while SANS cannot. Changes in $R_h$ measured by DLS, therefore, may correspond to changes in solvent interactions, while changes in $R_g$ measured by SANS may correspond to change in the polymer structure itself. The increase in $R_h$ with temperature, therefore, may correspond to an increase in solvent−polymer chain interactions. An increase in solvation is also suggested by a leveling off of the scattering intensity with temperature in the DLS measurements (Figure S4). Scattering intensity typically increases with $R_h$ unless there is a change in the refractive index of the polymer. The leveling off of scattering intensity corresponding to an increase in $R_h$ shown in Figure S4 suggests a decrease in the refractive index of the polymer due to solvent swelling.[32] However, PAMA and Star have similar polarities and backbones, and the dissimilar behavior is surprising. One would expect that polymers with higher polarity than the solvent (baseoil, in this case hexadecane) will respond in an equivalent manner to heat and have similar VIs. The VI values of the PAMA and Star are in the ballpark, but the observed DLS and SANS behavior is not.

It is important to note that we did not observe a Porod exponent of 3, characteristic of a collapsed polymer coil, for any polymer at all temperature conditions studied. Our temperature

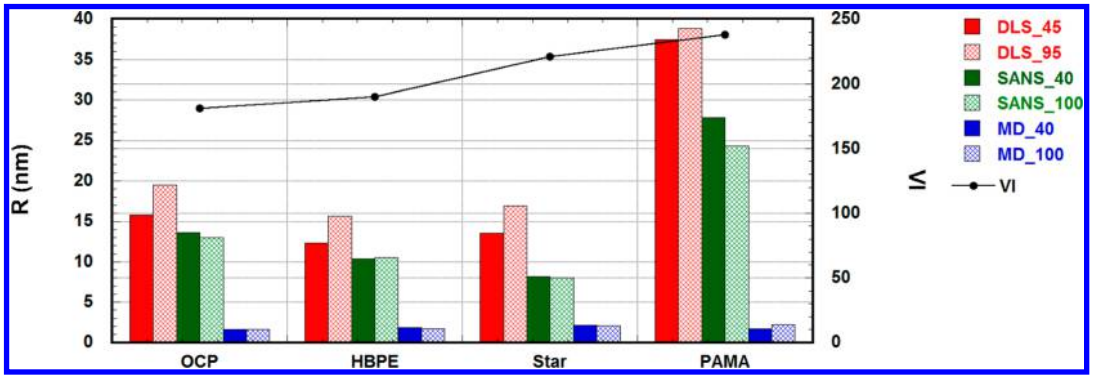


**Figure 3.** Comparison between DLS, SANS, and MD simulations results of polymers, along with the VI values. Here $R$ represents $R_h$ values from DLS, $R_g$ values from MD simulations, $R_g$ values for OCP and PAMA, and $L_c$ values for HBPE and Star polymers from SANS measurements.



DOI: 10.1021/acs.iecr.6b03812
Ind. Eng. Chem. Res. 2016, 55, 12983−12990

dependent viscosity measurements suggest that there is a significant improvement in the VI of 4Y oil, from 127, on adding all the above polymers as VIIs (Table 1). Interestingly, the PAMA polymer shows the greatest improvement in VI (238) despite showing a modest increase in $R_h$ with temperature through DLS measurements and a decrease in $R_g$ with temperature through SANS measurements. On the other hand, the HBPE and OCP polymers underwent a similar increase in $R_h$ with increasing temperature and demonstrated comparable VI performance (OCP − 181, HBPE − 190), even though a decrease in size with increasing temperature in SANS measurements was observed for OCP. Moreover, the Star polymer which showed a large increase in size through DLS but negligible change in size in SANS measurements had a VI of 221 slightly lower than that of the PAMA polymer, 238. These conflicting dimensional-performance behaviors can be observed clearly in Figure 3. Overall, the physical data obtained from DLS and SANS when qualitatively compared to empirically calculated VI values suggests that the current polymer globule-to-coil transition or coil expansion VI structure-performance relationship explanation is not all-telling, at least between 40 and 100 °C.

If polymer size changes do not correlate with VIs, other factors must be important in controlling the VIs of polymeric additives. The authors are well aware that molecular weight correlates well with thickening efficiency and generally with VIs, but this discussion is outside the scope of this study. HBPE and Star were prepared and analyzed in-house; however, OCP and PAMA were acquired through industrial partnerships, and their respective molecular weights are proprietary information. As described earlier, the VIIs investigated in this study have unique chemical compositions and architectures compared to one another. In particular, OCP and HBPE have different topologies but are roughly the same chemically, which translates to comparable KVs and subsequent VIs. The Star and PAMA additives have the highest VIs even though their architectures are very different from one another. Both of these additives have similar chemical compositions involving a polar ester backbone with lipophilic alkyl side chains. The polar backbone appears to have a role in increasing the VI by affecting polymer stiffness or solvent interactions.

## 5. CONCLUSIONS

Comparing the results from our two experimental techniques and MD simulations, it is clear that, while these techniques are excellent probes for polymer−solvent interactions, polymer size, and structure, they might not be able to predict the behavior of the polymers as VIIs in oil. The interactions of VIIs with oil include a complex mix of inter- and intramolecular interactions such as polar/nonpolar interactions that are long-range and not accounted for by the above techniques. The molecular weight, architecture, and chemical composition of the polymers have a huge influence on the solution viscosity and thermoresponsiveness.[33,34] Moreover, the topology and architecture of the VIIs have nonuniformities in them. We observed that polymers which significantly improve the VI (PAMA) do not show considerable change in size in the observation window between 40 and 100 °C. In conclusion, changes in polymer size do not significantly affect VI values as described by the traditional model suggesting that other factors are important in controlling and optimizing VI.

## ■ ASSOCIATED CONTENT

### Supporting Information

The Supporting Information is available free of charge on the ACS Publications website at DOI: 10.1021/acs.iecr.6b03812.

Figure S1, general structures and architectures of molecules under study; Figure S2, configuration of one of the analogs in nonpolar solvent and histogram of the calculated radius of gyration at two temperatures; Figure S3, SANS data with polymer excluded volume fit and correlation length model fit; Figure S4, example of DLS scattering intensity for one of the analogs; Table S1, fit results for polymer excluded volume fits and correlation length fits to the SANS data for the polymers (PDF)

## ■ AUTHOR INFORMATION


### Corresponding Author

*E-mail: lelia.cosimbescu@pnnl.gov.

### ORCID

Lelia Cosimbescu: 0000-0003-3055-4867

### Present Addresses

‖Energy Technologies and Materials Division, University of Dayton Research Institute, 300 College Park, Dayton, OH 45469-0076, USA.

⊥USDA, Agricultural International Service, 4700 River Rd, Riverdale, MD 20737.


### Author Contributions

The manuscript was written through contributions of all authors. All authors have given approval to the final version of the manuscript. P.B. contributed to the original concept and performed DLS measurements. S.K. conducted all SANS experiments and analysis. U.S.R. and A.M. conducted MD simulations. B.J.T. generated and analyzed DLS data. J.W.R. synthesized and characterized the materials and measured viscosities. L.C. proposed the original concept and original material design, structured collaborations, and analyzed results. All authors contributed to the writing of this manuscript.

### Notes

The authors declare no competing financial interest.

## ■ ACKNOWLEDGMENTS

P.B. is grateful for support from a Linus Pauling Distinguished Postdoctoral Fellowship at PNNL. This work utilized facilities supported in part by the National Science Foundation under Agreements DMR-0944772. U.S.R. and A.M. were supported by the U.S. Department of Energy's (DOE) Office of Vehicle Technology (under Contract No. 27029) of the PNNL AOP project. PNNL is a multiprogram national laboratory operated by Battelle for DOE under Contract DEAC05-76RL01830. U.S.R. and A.M. also acknowledge the American Chemical Society Petroleum Research Fund (# 55026-ND6) for partial support of this research. The computational aspects of this work used the Extreme Science and Engineering Discovery Environment (XSEDE), which was supported by National Science Foundation Grant No. ACI-1053575. The authors cordially acknowledge helpful discussions with Sona Slocum on similar work performed at Lubrizol. We thank Afton Chemical for generously donating base oils for screening purposes and both Lubrizol and Evonik for donating benchmark polymers (OCP and PAMA).



DOI: 10.1021/acs.iecr.6b03812
Ind. Eng. Chem. Res. 2016, 55, 12983−12990

## REFERENCES


(1) Van Horne, W. L. Polymethacrylates as Viscosity Index Improvers and Pour Point Depressants. *Ind. Eng. Chem.* **1949**, *41*, 952−959.

(2) Wang, J. L.; Ye, Z. B.; Zhu, S. P. Topology-Engineered Hyperbranched High-Molecular-Weight Polyethylenes as Lubricant Viscosity-Index Improvers of High Shear Stability. *Ind. Eng. Chem. Res.* **2007**, *46*, 1174−1178.

(3) Stöhr, T.; Eisenberg, B.; Müller, M. A. New Generation of High Performance Viscosity Modifiers Based on Comb Polymers. *SAE Int. J. Fuels Lubr.* **2009**, *1*, 1511−1516.

(4) Sutton, M. R.; Barton, W. R. S.; Price, D. Lubricating Composition Comprising Poly (isobutylene)/poly(vinyl aromatic) Block Copolymer. (2012) Int. Pat. 2,012,162,207.

(5) Johnson, J. R.; Schober, B. J. (The Lubrizol Corporation). (2014) Loose Core Star Polymers and Lubricating Composition Thereof, Int. Pat. 2,014,031,154.

(6) Duggal, A. (2012) Lubricant Additive. U.S. Pat. 2,012,010,1017 A1.

(7) Bruson, H. A. (1937) (Haas Company). Composition of Matter and Process, U.S. Pat. 2,091,627 A.

(8) Covitch, M. J.; Trickett, K. J. How Polymers Behave as Viscosity Index Improvers in Lubricating Oils. *Adv. Chem. Eng. Sci.* **2015**, *5*, 134−151.

(9) Mary, C.; Philippon, D.; Lafarge, L.; Laurent, D.; Rondelez, F.; Bair, S.; Vergne, P. New Insight into the Relationship Between Molecular Effects and the Rheological Behavior of Polymer Thickened Lubricants Under High Pressure. *Tribol. Lett.* **2013**, *52*, 357−369.

(10) Flory, P. J. In *Principles of Polymer Chemistry*, 1st ed.; Cornell University Press: Ithaca, NY, 1952; Chapter 14, p 622.

(11) Han, C. C. Molecular Weight and Temperature Dependence of Intrinsic Viscosity of Polymer Solutions. *Polymer* **1979**, *20*, 1083−1086.

(12) Colby, R. H. Scaling Analysis of the Temperature Dependence of Intrinsic Viscosity. *J. Polym. Sci., Part B: Polym. Phys.* **1997**, *35*, 1989−1991.

(13) Novotny, V. J. Temperature Dependence of Hydrodynamic Dimensions of Polystyrenes in Cyclohexane by Quasielastic Light Scattering. *J. Chem. Phys.* **1983**, *78*, 183−189.

(14) Mazur, J.; McIntyre, D. The Determination of Chain Statistical Parameters by Light Scattering Measurements. *Macromolecules* **1975**, *8*, 464−476.

(15) Melnichenko, Y. B.; Kiran, E.; Heath, K.; Salaniwal, S.; Cochran, H. D.; Stamm, M.; Hook, W. A. V.; Wignall, G. D. In *Scattering from Polymers*; Cebe, P., Hsiao, B. S., Lohse, D. J., Eds.; ACS Symposium Series, WA, 1999; Vol. *739*, p 317.

(16) Melnichenko, Y. B.; Wignall, G. D.; Van Hook, W. A.; Szydlowski, J.; Wilczura, H.; Rebelo, L. P. Comparison of Inter- and Intramolecular Correlations of Polystyrene in Poor and Theta Solvents via Small-Angle Neutron Scattering. *Macromolecules* **1998**, *31*, 8436−8438.

(17) Dong, Z. M.; Ye, Z. B. Hyperbranched Polyethylenes by Chain Walking Polymerization: Synthesis, Properties, Functionalization, and Applications. *Polym. Chem.* **2012**, *3*, 286−301.

(18) Robinson, J. W.; Zhou, Y.; Qu, J.; Erck, R.; Cosimbescu, L. Effects of Star-Shaped Poly(alkyl methacrylate) Arm Uniformity on Lubricant Properties. *J. Appl. Polym. Sci.* **2016**, *133*, 43611−43621.

(19) Dortmund Data Bank. http://www.ddbst.com/en/EED/PCP/VIS_C516.php (accessed August 4, 2016).

(20) Glinka, C. J.; Barker, J. G.; Hammouda, B.; Krueger, S.; Moyer, J. J.; Orts, W. J. The 30 m Small-Angle Neutron Scattering Instruments at the National Institute of Standards and Technology. *J. Appl. Crystallogr.* **1998**, *31*, 430−445.

(21) Kline, S. R. Reduction and Analysis of SANS and USANS Data Using IGOR Pro. *J. Appl. Crystallogr.* **2006**, *39*, 895−900.

(22) Benoit, H. The Diffusion of Light by Polymers Dissolved in a Good Solvent. *Comptes Rendus* **1957**, *245*, 2244−2247.

(23) Hammouda, B. SANS from Homogeneous Polymer Mixtures: A Unified Overview. *Adv. Polym. Sci.* **1993**, *106*, 87−133.

(24) Hammouda, B.; Ho, D. L.; Kline, S. R. Insight into Clustering in Poly(ethylene oxide) Solutions. *Macromolecules* **2004**, *37*, 6932−6937.

(25) Plimpton, S. Fast Parallel Algorithms for Short-Range Molecular Dynamics. *J. Comput. Phys.* **1995**, *117*, 1−19.

(26) Jorgensen, W.; Maxwell, D.; Tirado-Rives, J. Development and Testing of the OPLS All-Atom Force Field on Conformational Energetics and Properties of Organic Liquids. *J. Am. Chem. Soc.* **1996**, *118*, 11225−11236.

(27) Ye, X.; Cui, S.; de Almeida, V. F.; Khomami, B. Effect of Varying the 1−4 Intramolecular Scaling Factor in Atomistic Simulations of Long-Chain n-alkanes with the OPLS-AA Model. *J. Mol. Model.* **2013**, *19*, 1251−1258.

(28) Ramasamy, U. S.; Lichter, S.; Martini, A. Effect of Molecular-Scale Features on the Polymer Coil Size of Model Viscosity Index Improvers. *Tribol. Lett.* **2016**, *62*, 1−7.

(29) Flory, P. J. In *Principles of Polymer Chemistry*, 1st ed.; Cornell University Press, Ithaca, NY, 1952; Chapter 14, p 601.

(30) Aichmayer, B.; Margolis, H. C.; Sigel, R.; Yamakoshi, Y.; Simmer, J. P.; Fratzl, P. The Onset of Amelogenin Nanosphere Aggregation Studied by Small-Angle X-Ray Scattering and Dynamic Light Scattering. *J. Struct. Biol.* **2005**, *151*, 239−249.

(31) Ramasamy, U. S.; Lichter, S.; Martini, A. Effect of Molecular-Scale Features on the Polymer Coil Size of Model Viscosity Index Improvers. *Tribol. Lett.* **2016**, *62*, 1−7.

(32) Han, F.; Soeriyadi, A. H.; Vivekchand, S. R. C.; Gooding, J. J. Simple Method for Tuning the Optical Properties of Thermoresponsive Plasmonic Nanogels. *ACS Macro Lett.* **2016**, *5*, 626−630.

(33) Cheng, H.; Xie, S.; Zhou, Y.; Huang, W.; Yan, D.; Yang, J.; Ji, B. Effect of Degree of Branching on the Thermoresponsive Phase Transition Behaviors of Hyperbranched Multiarm Copolymers: Comparison of Systems with LCST Transition Based on Coil-to-Globule Transition or Hydrophilic−Hydrophobic Balance. *J. Phys. Chem. B* **2010**, *114*, 6291−6299.

(34) Tian, W.; Wei, X.-Y.; Liu, Y.-Y.; Fan, X.-D. A Branching Point Thermo and pH Dual-Responsive Hyperbranched Polymer Based on Poly(N-vinylcaprolactam) and Poly(N,N-diethyl aminoethyl methacrylate). *Polym. Chem.* **2013**, *4*, 2850−2863.




DOI: 10.1021/acs.iecr.6b03812
*Ind. Eng. Chem. Res.* 2016, 55, 12983−12990